SEPARATION OF TONAL AND BROADBAND NOISE COMPONENTS BY CYCLOSTATIONARY ANALYSIS OF THE MODAL SOUND FIELD IN A LOW-SPEED FAN TEST RIG

Maximilian BEHN, Benjamin PARDOWITZ,
Ulf TAPKEN

German Aerospace Center (DLR), Institute of Propulsion Technology,
Engine Acoustics Department, Müller-Breslau-Straße 8,
10623 Berlin, Germany

SUMMARY

The radial mode analysis is a well-established method used to analyze the tonal and broadband components of in-duct sound fields radiated from axial turbomachinery. Based on the cyclostationary analysis, a separation procedure is presented in order to obtain the signals associated with the tonal and broadband sound fields separately. The analysis of experimental data shows that the sound power and the mode coherences of the respective sound field components are identified exactly. Furthermore, the cyclostationary analysis is used to track the development of the sound power as a function of the rotor rotation angle at the blade passing frequencies, exemplarily.

INTRODUCTION

The development of axial turbomachinery such as ventilators and aero engines imposes increasing requirements regarding a reduction of the radiated tonal and broadband sound. In many applications the in-duct sound fields are sensed using wall-flush mounted microphone arrays in order to minimize the influence of the sensor installations on the sound field. The analysis of tonal sound field components can be performed by use of the radial mode analysis [1-6], which allows the determination of the sound power of all cut-on modes. Recently, the application of the radial mode analysis to determine broadband mode amplitudes for experimental data from a laboratory low-speed fan test rig was presented [7]. The method assumes that the broadband sound field can be modelled as a quasi-stationary process, i.e. the fan noise sources generate an invariant mean broadband sound field with statistical evidence. In broadband sound analysis typically the contributions of tonal components are filtered by convolution of the original spectrum with a

Gaussian window function, which sometimes is referred to as ‘tone-cutting method’, cp. [8]. The method assumes that the broadband spectrum does not feature sharp peaks and the method acts as a smoothing filter on the considered spectrum.

In this study, another approach is investigated. It is based on the assumption that the statistical properties of the broadband sound field are periodic in time and directly related to the rotor revolution, i.e. the assumption of a cyclostationary process [9]. In contrast to the quasi-stationary analysis, the cyclostationary analysis allows the separation of the measured pressure signal into a deterministic signal and a random signal, which are interpreted as the tonal respectively the broadband signal components. The separation procedure preserves the amplitude and phase relations of the respective signal components.

The article has two main objectives. The first objective is to analyze the effect of the signal separation procedure on the resulting mode sound powers and mode coherences. The results are compared to the outcome of the Full Sensor Array (FSA) method [10], which was proposed as a reference method by Tapken et al. [7]. Experimental data measured at a laboratory low-speed fan test rig is used as the basis for the comparison.

The second objective is to examine the potential benefits of the cyclostationary analysis for the development of a source localization technique for rotating sources. Based on the cyclostationary analysis the Wigner-Ville spectrum [11] is computed, which describes the instantaneous development of the statistical signal properties such as auto- and cross-power spectra with respect to the rotor revolution. The method is assessed by evaluating the instantaneous mode sound power as a function of the rotation angle at the first and second blade passing frequencies.

EXPERIMENTAL SETUP

The laboratory fan test rig is shown in Fig. 1. Its total length is approximately 8 m. At the inlet section, a turbulence control screen (not shown in the figure) and a bellmouth nozzle are installed. The outer radius at the fan stage section is 226.8 mm. The rotor is equipped with 18 blades and the stator has 32 vanes resulting in a cut-off design regarding the first blade passage frequency. At the outlet section, an anechoic duct termination and a throttle are installed in order to minimize acoustic reflections respectively to adjust the mass flow and hence the aerodynamic operating condition of the rotor. All results shown in the present study are given for a rotor shaft frequency of 50 Hz and at an operation condition with reduced mass flow $\dot{m}_{red} = 2.53\ kg/s$ and fan pressure ratio $\pi = 1.0140$.

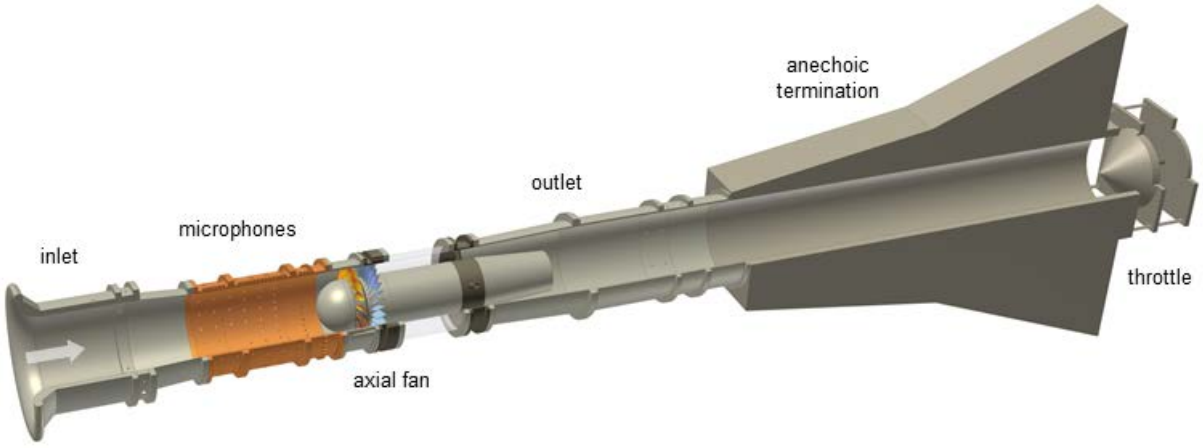

Figure 1: Overview of the laboratory low-speed fan test rig. The fan stage is equipped with 18 rotor blades and 32 stator vanes. Acoustic measurements are performed by use of the microphone array in the inlet section.

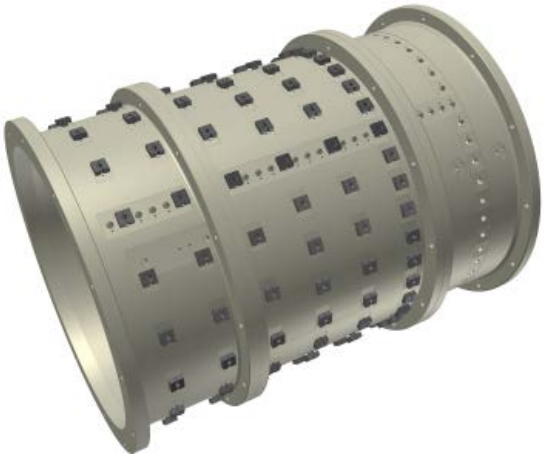

Figure 2: Microphone array equipped with 138 sensors (shown in black).

Upstream of the axial fan stage, a microphone array equipped with 138 sensors is used to measure the sound field radiated from the fan. The microphone array section is illustrated in Fig. 2. The sensors are distributed in six uniform ring arrays at equidistant axial spacing. Sorted in the direction of the flow, the sensor count per ring array are 18 sensors for the first three rings, 24 sensors for rings 4 and 5, and 36 sensors for ring 6. Sound pressure signals were recorded using a sampling rate f_s of 65.536 kHz and measurement duration of 60 s.

SEPARATION OF TONAL AND BROADBAND SIGNAL COMPONENTS

The measured time series were recorded at a constant sampling rate. In order to decompose the measured signal into a deterministic and a random signal, both being directly related to the rotor revolution, the measured signal is resampled with respect to the rotor shaft trigger. In this study the raw signal is resampled using linear interpolation. In the following, the resampled signal is denoted the total signal $p(t)$. Subsequently, the signal is divided into blocks, with each block having a length of 16 rotor revolutions. The ensemble average of these blocks yields the deterministic signal component $s(t)$, which can be interpreted as the tonal signal components. The residual signal $r(t) = p(t) - s(t)$ embodies the random signal components, which describe the broadband signal components of the measured signal. The deterministic signal component comprises first-order cyclostationarity (CS1) [9], i.e. $s(t) = s(t+T)$ with T the time period of one rotor revolution, and the random signal component is second-order stationary (CS2), i.e. $R_{rr}(t,\tau) = R_{rr}(t,\tau+T)$ with the instantaneous autocorrelation function:

$$R_{rr}(t,\tau) = \frac{1}{T_{meas}} \int_{t_m=0}^{T_{meas}} r(t_m - \tau)\, r(t_m + \tau)\, dt_m. \qquad (1)$$

Here T_{meas} is the total measurement duration and t_m is the variable for the measurement time. It should be noted, that the definition of the instantaneous autocorrelation function differs from the definition by Antoni [11] regarding the factor ½ applied to the time lag τ.

Figure 3 shows the average auto-power spectra of all sensors for the total measured pressure signals and the first- and second-order cyclostationary signal components. The separation of the CS1- and CS2-signal components yields an overall 20 dB level difference between both signal components. The CS1 component features peaks at the engine order components with a base frequency of 50 Hz, particularly, the blade passing frequencies BPF1 at 900 Hz and BPF2 at 1800 Hz. At BPF1, the CS1- and CS2-signal components are almost equally strong. Further investigations are needed to clarify, why the BPF1 component is present with this configuration in despite of the cut-off design

of the fan stage. Tapken et al. [7] explain that the occurrence of the BPF1 component can be caused by an inhomogeneous, incoming turbulent flow field (although a TCS was used) or flow separation at the rotor hub. At BPF2, the CS1- and CS2-signal components show a level difference of about 20 dB.

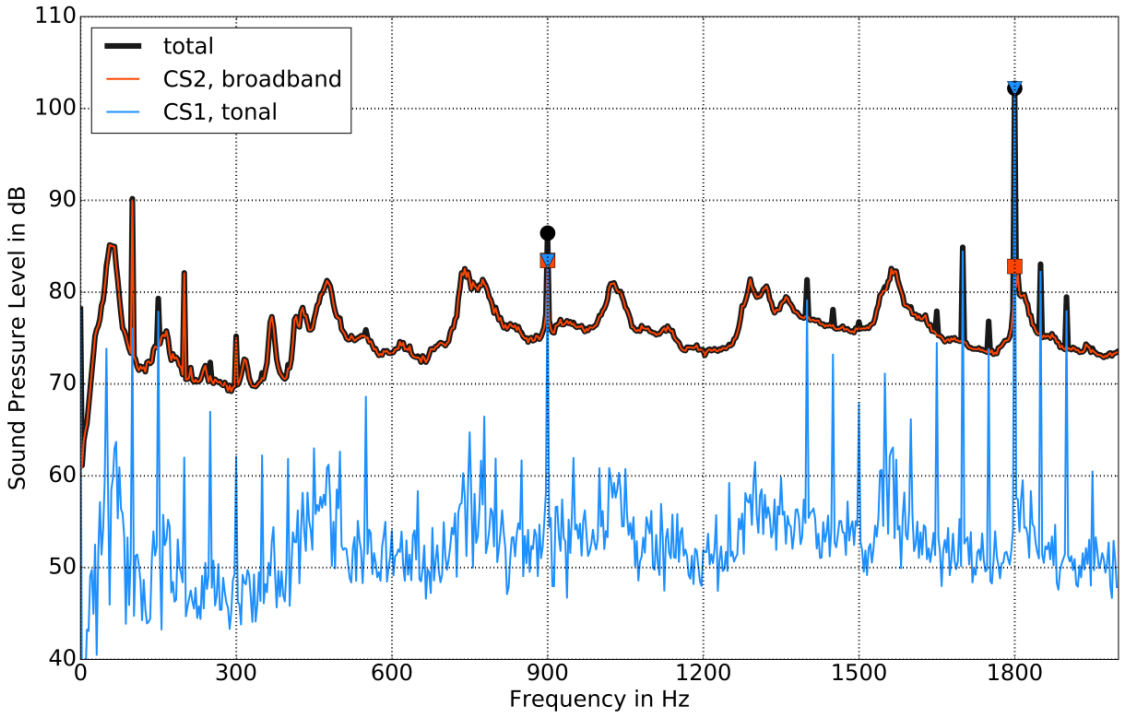

Figure 3: Average auto-power spectra for the total measured pressure signals (black, circle) and the first-(blue, triangle) respectively second-order (red, square) cyclostationary components after the application of the signal separation procedure. Markers are placed at the blade passing frequencies.

RADIAL MODE ANALYSIS OF SOUND FIELDS IN ANNULAR FLOW DUCTS

The acoustic field inside the flow duct can be described by an infinite series of radial modes, which is obtained from the general solution of the convective Helmholtz equation in cylindrical coordinates [5]:

$$p(x,r,\varphi) = \sum_{m=-\infty}^{\infty}\sum_{n=0}^{\infty}\left(A_{mn}^{+}e^{ik_{mn}^{+}x} + A_{mn}^{-}e^{ik_{mn}^{-}x}\right) f_{mn}(r)\, e^{im\varphi}, \qquad (2)$$

with the radial mode shape function $f_{mn}(r)$ and the axial wave numbers $k_{mn}^{\pm}$. The radial mode shape function $f_{mn}(r)$ is composed of the sum of the Bessel functions of first and second kind and order m. The complex mode amplitudes are denoted by A_{mn}^{+} for the downstream propagating and A_{mn}^{-} for the upstream propagating mode of azimuthal and radial mode order (m,n). The sound field model assumes incompressible and isentropic flow, a constant axial mean flow profile, and stationary mean temperature and density.

For the CS1 components, the mode amplitudes $\mathbf{a} = \left(A_{-m_{max}n_{max}}^{+}, \cdots, A_{00}^{+}, A_{00}^{-}, \cdots, A_{m_{max}n_{max}}^{-}\right)$ are determined by solving a system of linear equations using a set of averaged measured sound pressure signals $\mathbf{p} = \left(p(x_0, r_0, \varphi_0, \omega), \cdots, p\left(x_{N_{Mic}}, r_{N_{Mic}}, \varphi_{N_{Mic}}, \omega\right)\right)$ [5]:

$$\mathbf{p} = \mathbf{W}\mathbf{a} \qquad (3)$$

with $\mathbf{W}$ the matrix of mode transfer functions. The matrix entries of $\mathbf{W}$ are the individual terms of the sum given in Eq. (2). In this case, it is assumed that the modes are coherent among each other and with the sources, respectively.

The broadband sound field components (CS2) are treated differently. Due to the random nature of the CS2-signals the appropriate statistical description of the mode amplitudes is given in terms of mean values and spatial cross-coherences. As a result, the cross-spectral matrix of the mode amplitudes $\mathbf{S_{aa}} = \lim_{T_{meas}\to\infty} E\{\mathbf{aa^H}\}$ follows from inversion of the following equation [10]:

$$\mathbf{S_{pp}} = \mathbf{W}\mathbf{S_{aa}}\mathbf{W^H}, \tag{4}$$

where $E\{\cdot\}$ is the expected value, $\mathbf{S_{pp}}$ is the cross-spectral matrix of the pressure signals, and $(\cdot)^{\mathbf{H}}$ is the Hermitian operator. Since the method is explicitly formulated for sound fields of arbitrary mode coherences, it is also suited for the analysis of tonal components.

The linear system of eq. (3) and (4) both are solved using the pseudo-inverse $\mathbf{W}^+ = \left[\mathbf{W^H W}\right]^{-1}\mathbf{W^H}$ **(**cp. references [5] and [10]**)**. After the mode amplitudes are determined, the sound power associated to each individual mode can be calculated by

$$\langle P_{mn}^{\pm}\rangle = \frac{\pi R^2}{\rho c}\frac{\alpha_{mn}\left(1-M_x^2\right)^2}{\left(1\mp\alpha_{mn}M_x\right)^2}\langle|A_{mn}^{\pm}|^2\rangle \tag{5}$$

with $\left\langle\left|A_{mn}^{\pm}\right|^2\right\rangle$ the auto-power spectrum of mode amplitude and α_{mn} the mode cut-on factor (see e.g. reference 5). The summed sound power over all radial modes of the same azimuthal mode order transported in each direction is calculated as $\left\langle P_m^{\pm}\right\rangle = \sum_n \left\langle P_{mn}^{\pm}\right\rangle$. Summation of $\left\langle P_m^{\pm}\right\rangle$ over all azimuthal mode order yields $\left\langle P^{\pm}\right\rangle = \sum_m \left\langle P_m^{\pm}\right\rangle$.

Based on the cross-spectral matrix of the mode amplitudes the coherence between pairs of modes is given as

$$\gamma_{mn}^{\mu\nu} = \frac{\left|\left\langle A_{mn}{A_{\mu\nu}}^*\right\rangle\right|^2}{\left\langle\left|A_{mn}\right|^2\right\rangle\left\langle\left|A_{\mu\nu}\right|^2\right\rangle}\,. \tag{6}$$

The accuracy of the mode decomposition according to eq. (3) and (4) using the microphone array shown in Fig. 2 was evaluated by means of a matrix condition analysis [7]. As a result, the mode decomposition is accurate up to a frequency of 2000 Hz.

ANALYSIS OF THE INFLUENCE OF SEPARATION PROCEDURE ON THE OUTCOME OF THE RADIAL MODE ANALYSIS

The CS1 components $s(t)$ are used as input to the radial mode analysis according to eq. (3). The total signals $p(t)$ and the CS2 components $r(t)$ are analyzed using the FSA method according to eq. (4). The summed sound power over all cut-on modes propagating downstream and upstream $\left\langle P^{\pm}\right\rangle$ are shown in Fig. 4 for the total and the separated signals. The results show, that the determined sound powers using the total signals matches the sum of both signal components, CS1 and CS2. In contrast to the result obtained with application of the ‘tone-cutting method’ as conducted by Enghardt et al. [8], the CS2 sound power spectrum features significant peaks at the blade passing frequencies, particularly at BPF1. The presence of inflow distortions is a possible

reason for the occurrence of such peaks in broadband (CS2) sound power spectra. Another interesting aspect is the presence of the multiple peaks of the CS1 components around BPF2. The results prove that these components originate from fully correlated sources. Presumably, variations of the individual rotor wakes cause the presence of these sources [12]. In general, this demonstrates the benefit for the detailed analysis of the noise generation mechanisms, since the tonal (CS1) and broadband (CS2) sound field components are typically associated to different noise sources.

Figure 5 shows the evaluation of the mode coherence for the upstream modes of azimuthal mode order $m = 0$ with all other cut-on modes. The modal field determined using the CS2 signal components features the same large coherence between the modes with the same azimuthal mode order $m = 0$ as is determined using the total signals. It should be noted that at the blade passing frequencies and other engine order components the increased coherences with modes having a different azimuthal mode order found in the analysis of the total signal are not present in the analysis using the separated signals. This is in good agreement with the assumption that the mode constituents of the tonal sound field components are coherent as they are associated to the first-order cyclostationary signal components and therefore not included in the results shown in Fig. 5b.

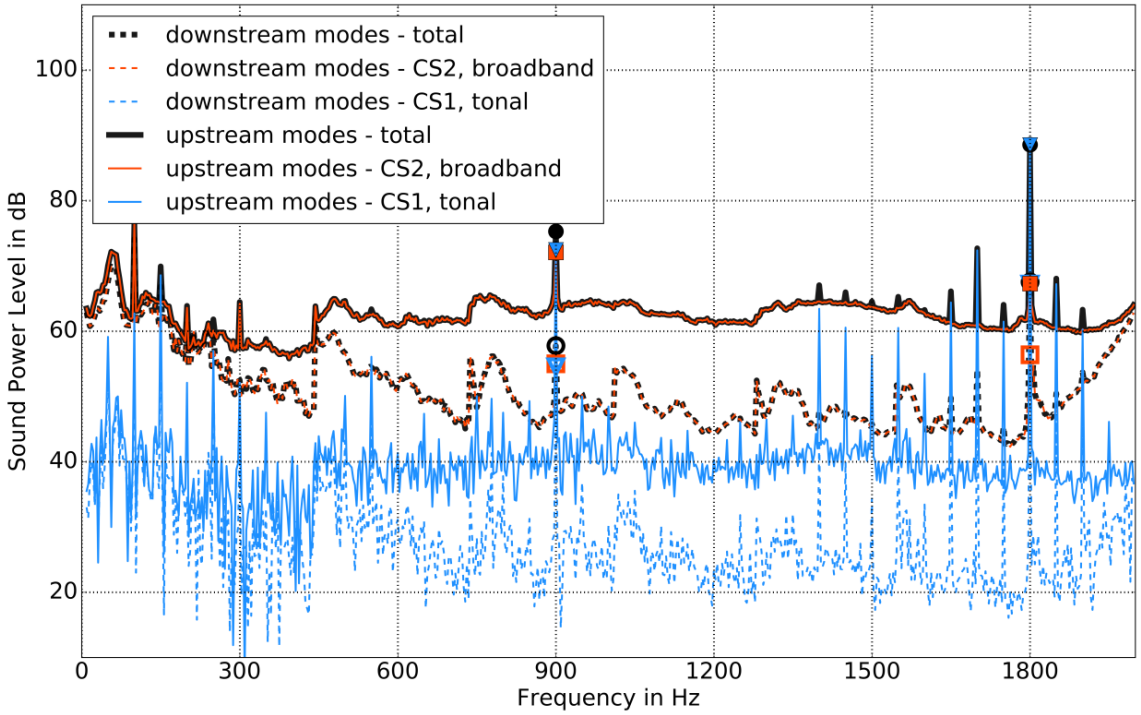

Figure 4: Total sound power of the upstream propagating modes and the downstream propagating modes determined using the total measured pressure signals (black, circle), the first-(blue, triangle) and the second-order (red, square) cyclostationary components. Markers are placed at the blade passing frequencies.

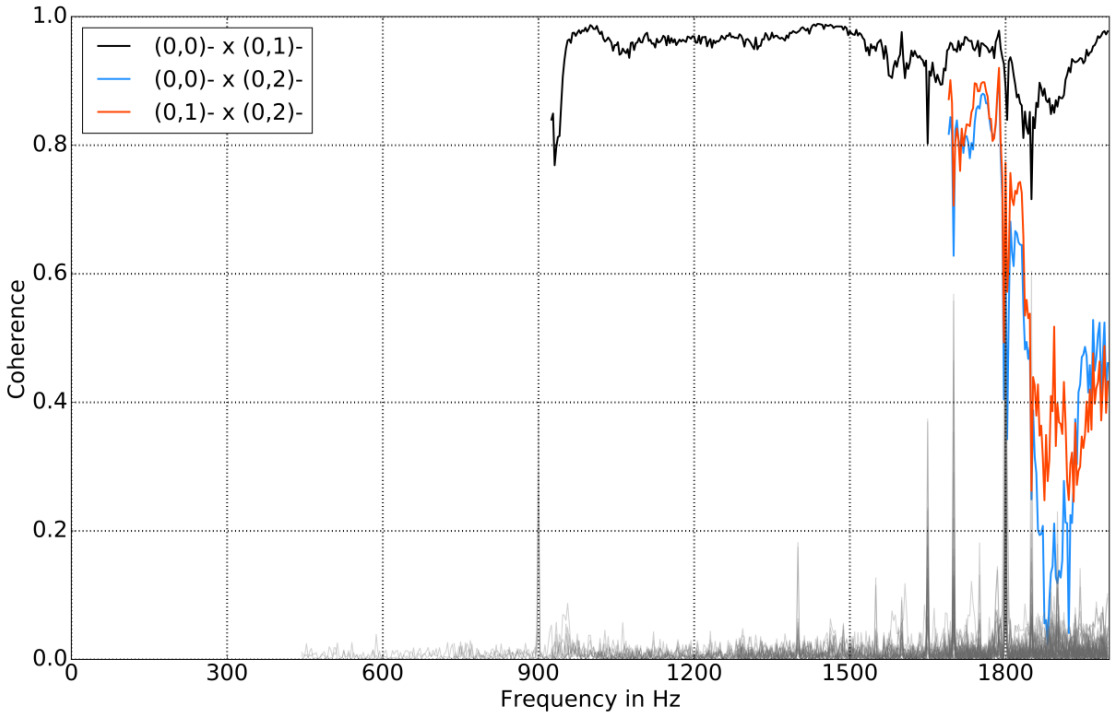

a) Results for the analysis using the total sensor signals.

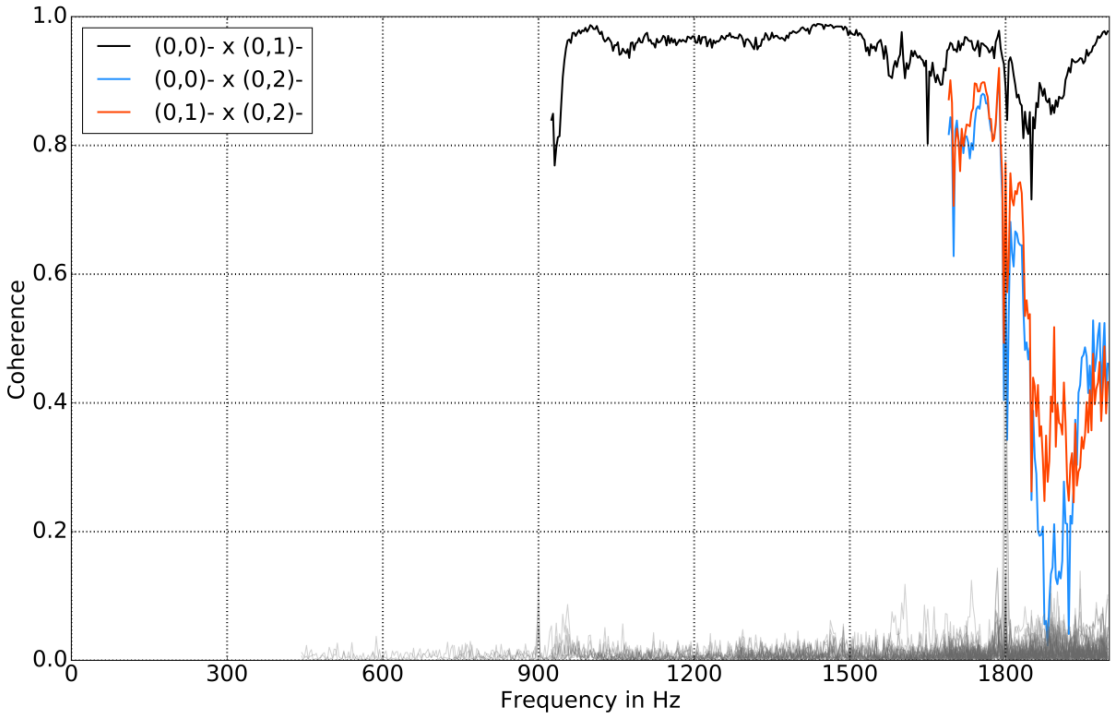

b) Results for the analysis using the second-order cyclostationary signal components

Figure 5: Mutual coherences of the upstream radiated mode $(0,0), (0,1)$ *and* $(0,2)$ *(shown in colored lines) and mutual coherences of the same modes with all other azimuthal mode orders* $m \neq 0$ *(shown in gray lines).*

CYCLOSTATIONARY SPECTRAL ANALYSIS USING THE WIGNER-VILLE SPECTRUM

In the scope of the cyclostationary spectral analysis, a useful tool is presented by Antoni [11] called the Wigner-Ville Spectrum, which yields the instantaneous auto- and cross-power spectra for signals being strongly correlated to periodic processes, e.g. the sound generation related to the rotation of a fan. Following Antoni [9], the Wigner-Ville spectrum can be determined using the autocorrelation function given in eq. (1) according to the following equation:

$$W_{rr}(t, f) = \underset{f_{cycle}\to t}{\mathrm{F}^{-1}}\left\{\overline{\underset{\tau\to f}{\mathrm{F}}\left\{\underset{t\to f_{cycle}}{\mathrm{F}}\left\{R_{rr}(t,\tau)\right\}\right\}}\right\}. \tag{7}$$

with $\underset{t\to f_{cycle}}{\mathrm{F}}$ indicating the Fourier transform with respect to the time variable t and the cyclic frequency variable f_{cycle}. $\underset{f_{cycle}\to t}{\mathrm{F}^{-1}}$ denotes the inverse Fourier transform. The operator $(\overline{\cdots})$ indicates the average over several rotor revolutions. Here the cyclic frequency f_{cycle} comprises the set of the fundamental cycle of the cyclostationary process and its integer harmonics, i.e. the first engine order and its harmonics. Due to the rotor-coherent resampling, the frequency variable f is given in terms of engine orders. In general, the frequency f and the cyclic frequency f_{cycle} extend over the same frequency range up to the Nyquist-frequency limit $\frac{f_s}{2}$. Taking into account that the cyclic frequency f_{cycle} can be interpreted as a modulation frequency of the frequency component f, it is useful to limit the range of cyclic frequencies considered in the calculation of the Wigner-Ville spectrum. In this study, the set of cyclic frequencies ranges from -5 EO to +5 EO. This range was determined from the stationary spectrum of the CS1-components shown in Fig. 3 in order to ensure that all modulation frequencies with significant strength are taken into account e.g. for BPF2.

Equation (7) can readily be applied to the CS1-signal components $s(t)$ as well as the CS2-signal components $r(t)$. The set of Wigner-Ville spectra calculated for all combinations of sensors in the sensor array is used as input to the radial mode analysis for the CS1 components and the FSA method for the CS2 components, which enables the determination of the mode spectrum and hence the sound power as a function of the rotor rotation angle.

In the following, the application of the Wigner-Ville spectra as input to the radial mode analysis is presented exemplarily for the CS2 components at BPF1 and for the CS1 components at BPF2. The first case is of interest because of the significant peak, which occurs for the CS2 component at BPF1. The analysis of the CS1 component at BPF2 is performed in order to obtain deeper insight into the noise generation due to rotor-stator interaction.

In Fig. 6, the resulting sound powers for the upstream propagating modes are shown for the CS2 sound field components at the first blade passing frequency. The angular position of the rotor is given relative to the shaft reference position at 0 degrees corresponding to the top dead center. The radiated mode spectrum does not feature any dominant modes due to the cut-off design of the fan stage. The instantaneous mode sound power varies by up to approximately 5 dB. In contrast to the modes with azimuthal mode orders $m = -1$ and $m = -2$, the sound power for the mode $m = 0$ decreases at the angular position of about 200 degrees. The modes with positive azimuthal mode order show smaller variations of the sound power than the modes with mode order $m \leq 0$.

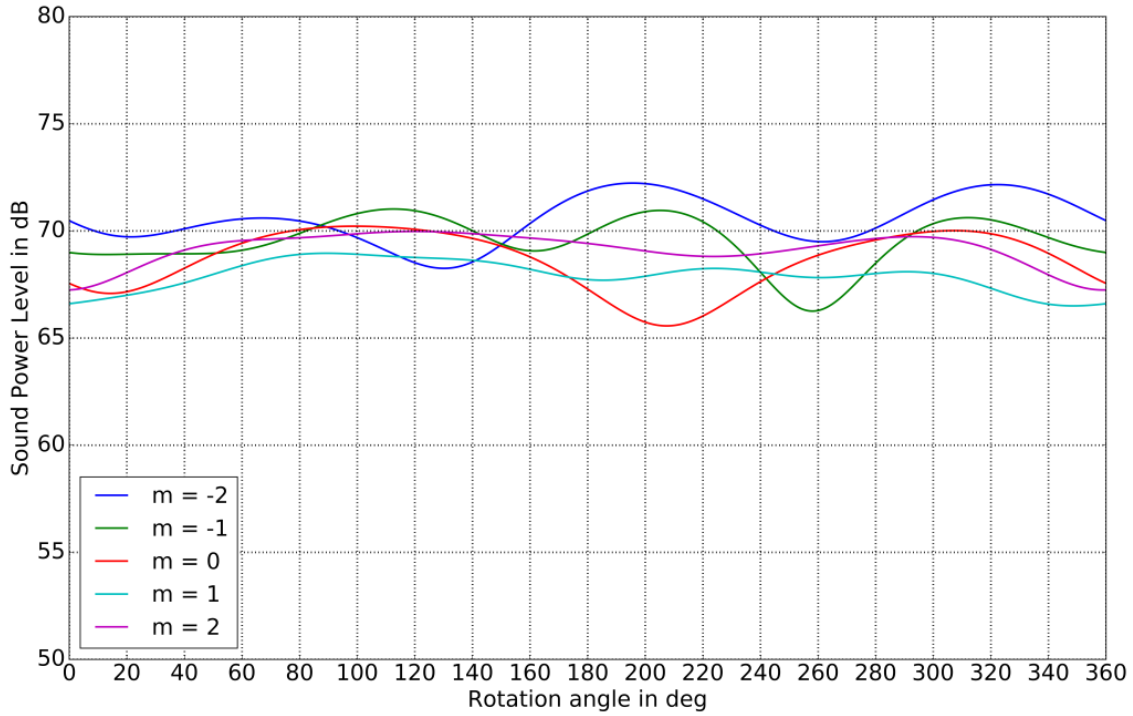

Figure 6: Development of the sound power $\langle P_m^- \rangle$ summed over all radial modes with respect to the azimuthal mode order for the upstream propagating modes over the rotor revolution. The Wigner-Ville spectra of the second-order cyclostationary signal components are used as input for the FSA method. The shaft reference position is at 0 degrees corresponding to the top dead center. The analysis is shown for the first blade passing frequency.

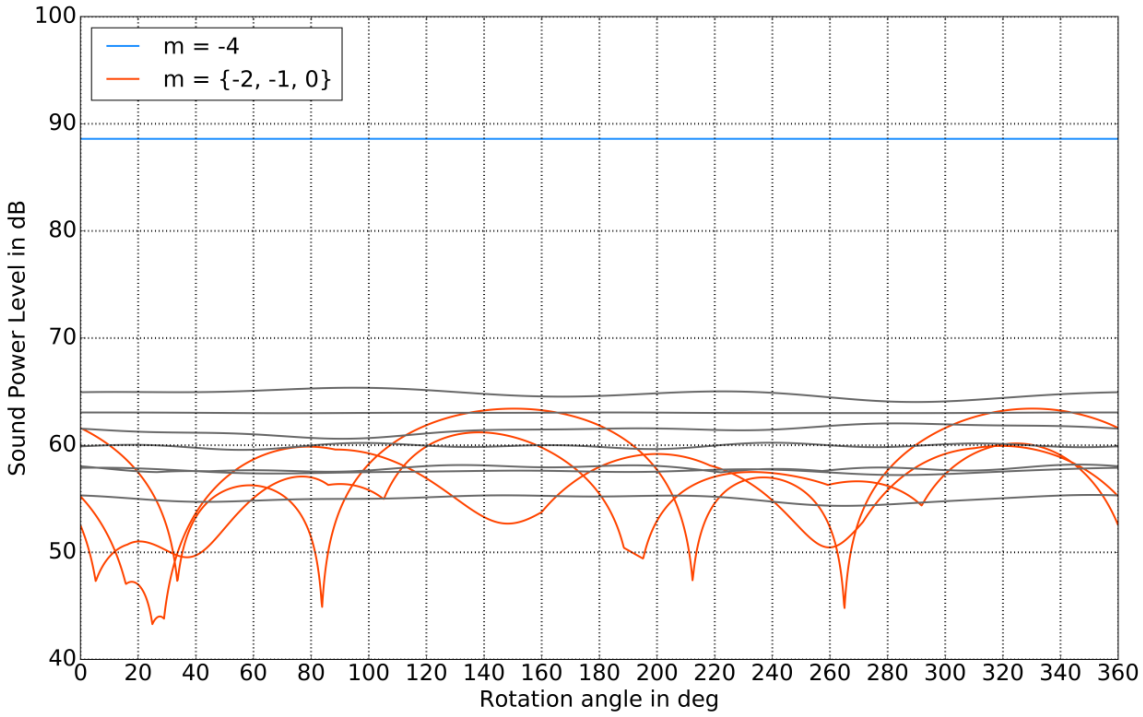

Figure 7: Development of the sound power $\langle P_m^- \rangle$ summed over all radial modes with respect to the azimuthal mode order over the rotor revolution. The Wigner-Ville spectrum of the first-order cyclostationary signal components is used as input to the radial mode analysis. The shaft reference position is at 0 degrees corresponding to the top dead center. The analysis is shown for the second blade passing frequency. The rotor-stator interaction mode has the azimuthal mode order $m = -4$.

Figure 7 presents the development of the radiated sound power propagating upstream for the CS1 sound field components at the second blade passing frequency. The rotor-stator interaction mode of order $m = -4$ is dominant by more than 20 dB and exhibits a constant sound power over the rotor revolution. This can be explained by the fact that for the given rotor blade and stator vane count and assuming a finite rotor wake width at least one pair of a single blade and vane interact at every rotor rotation angle. The other modes show stronger variations with respect to the rotor revolution. Particularly, the modes with low azimuthal mode orders $m = \{-2,-1,0\}$, whose rotational direction is in the direction of the rotor rotation, yield variations of the determined sound power by up to about 15 dB. This may be explained by the higher number of radial mode orders, which are cut-on for these modes. The higher radial mode orders can be expected to be more sensitive with respect to their excitation by changing radial distributions of the sound sources situated at the rotor and the stator as the rotor advances. The fact that only modes co-rotating with the rotor show this phenomenon can be explained by the rotor shielding effect [13]. The rotor shielding effect causes modes that rotate against the rotational direction of the rotor to attenuate as they are transmitted through the rotor blade row.

CONCLUSION

A procedure for separating the signal components associated with the tonal and broadband sound fields is presented based on the cyclostationary analysis. The separation preserves the phase and amplitude relations in the considered frequency range and allows the calculation of the sound power radiated by a low-speed fan for the respective sound field components. It is shown, that the inter-mode coherences are retained through the separation procedure.

Based on the cyclostationary analysis, the Wigner-Ville spectrum is determined for all combinations of sensors in the sensor array, which can be used as input to the radial mode analysis and therefore allows the calculation of the instantaneous sound power. The resulting variations of the mode sound power amount to about 5 to 15 dB for individual azimuthal mode orders depending on e.g. the number of cut-on radial mode orders.

The mode analysis based on the Wigner-Ville spectrum allows tracking the development of the mode spectrum over the rotor revolution. The instantaneous mode spectra and the instantaneous sound power may provide new insights into the noise generation mechanism of rotor-stator stages and will be used in the context of a source localization method to be developed in the future.

BIBLIOGRAPHY

[1] C. J. Moore – *Measurement of radial and circumferential modes in annular and circular fan ducts*, Journal of Sound and Vibration, Vol. 62, No. 2, pp. 235-256, **1979**

[2] P. D. Joppa – *Acoustic Mode Measurements in the Inlet of a Turbofan Engine*, Journal of Aircraft, Vol. 24, No. 9, pp. 587-593, **1987**

[3] L. Enghardt – *Experimental verification of a radial mode analysis technique using wall-flush mounted sensors*, Journal of the Acoustical Society of America, Vol. 105, Issue 2, pp. 1186, **1999**

[4] D. L. Sutliff – *Turbofan duct mode measurements using a continuously rotating microphone rake*, International Journal of Aeroacoustics, Vol. 6, No. 2, pp. 147-170, **2007**

[5] U. Tapken, L. Enghardt – *Optimization of Sensor Arrays for Radial Mode Analysis in Flow Ducts*, 12th AIAA/CEAS Aeroacoustics Conference, Cambridge, Massachusetts (USA), AIAA 2006-2638, **2006**

[6] P. Sijtsma, J. Zillmann – *In-Duct and Far-Field Mode Detection Techniques*, 13th AIAA/CEAS Aeroacoustics Conference, Rome, Italy, AIAA 2007-3439, **2007**

[7] U. Tapken, B. Pardowitz, M. Behn – *Radial Mode Analysis of fan broadband noise*, 23rd AIAA/CEAS Aeroacoustics Conference, Denver, Colorado (USA), AIAA 2017-3715, **2017**

[8] L. Enghardt, A. Moreau, U. Tapken, F. Kennepohl – *Radial Mode Decomposition in the Outlet of a LPT Turbine – Estimation of the Relative Importance of Broadband Noise*, 15th AIAA/CEAS Aeroacoustics Conference, Miami, Florida (USA), AIAA 2009-3286, **2009**

[9] J. Antoni – *Cyclostationarity by examples*, Mechanical Systems and Signal Processing, Vol. 23, pp. 987-1036, **2009**

[10] W. Jürgens, U. Tapken, B. Pardowitz, P. Kausche, G. J. Bennett, L. Enghardt – *Technique to Analyze Characteristics of Turbomachinery Broadband Noise Sources*, 16th AIAA/CEAS Aeroacoustics Conference, Stockholm (Sweden), AIAA 2010-3979, **2010**

[11] J. Antoni – *Cyclic spectral analysis in practice*, Mechanical Systems and Signal Processing, Vol. 21, pp. 597-630, **2007**

[12] L. Enghardt, A. Moreau, P. Kausche, T. Carolus – *Active Control of Fan Tones by means of Trailing Edge Blowing*, 21st AIAA/CEAS Aeroacoustics Conference, Dallas (USA), AIAA 2015-2828, **2015**

[13] J. B. H. M. Schulten – *Transmission of Sound through a Rotor*, 14th DGLR/AIAA Aeroacoustics Conference, Aachen (Germany), DGLR/AIAA 92-02-085, **1992**